Numerical investigation of light gas release, stratification and dissolution in TH22 test facility using 3-D CFD code GASFLOW-MPI

Guang Hu [a,*], *Fangnian Wang* [a], *Qingxin Ba* [a,b], *Jianjun Xiao* [a,**], *Thomas Jordan* [a]

[a] *Institute of Thermal Energy Technology and Safety, Karlsruhe Institute of Technology, Karlsruhe 76344, Germany*
[b] *Institute of Thermal Science and Technology, Shandong University, Jinan 250061, China*

GRAPHICAL ABSTRACT

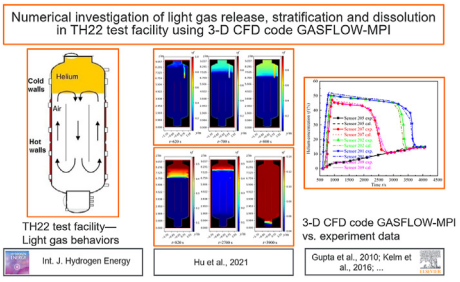

ARTICLE INFO

Keywords:
Light gas behaviors
Release and stratification
Dissolution
Hydrogen safety
GASFLOW-MPI

ABSTRACT

An accurate prediction of the hydrogen behaviors in the accident and management process is a crucial topic for both the hydrogen safety assessment and safety analysis in the confined enclosure like the containment of the nuclear power plant (NPP). Hence, the hydrogen behaviors including the transient light gas release, stratification and dissolution in the TH22 test facility for the NPP containment are analyzed and compared using the 3-D CFD code GASFLOW-MPI in this study. In this paper, the light gas helium is adopted as a substitute for the hydrogen in the calculations in accordance with the experiment. Firstly, the detached eddy simulation (DES) turbulence model, 3-D numerical model and experiment setup are introduced. Then, the hydrogen behaviors with the GASFLOW-MPI including the light gas release, stratification and dissolution are analyzed and validated with the experiment data. In addition, the velocity profiles, light gas concentrations, dimensionless numbers and temperature distributions are evaluated for the characteristics of the hydrogen behaviors. The results indicate that the calculation results agree well with the experiment data. Foremostly, the relative errors between the calculation results

* *Corresponding author.*
** *Corresponding author.*
E-mail addresses: guang.hu@kit.edu (G. Hu), jianjun.xiao@kit.edu (J. Xiao).

and experiment data during the phase of the dissolution of the light gas cloud are within 11.9%. Meanwhile, the relative errors of the time for the complete dissolution during the phase of the dissolution of the light gas cloud are within 5.0%. For the light gas release and stratification phase, the jet flow dominates as the Froude (Fr) number exceeds 10 during the time $t = 600$ s–800 s. Additionally, the time averaged centerline velocity and light gas concentration after the potential core region decay with a slop of 1/z which coincide with the theoretical jet limit. Lastly, the light gas concentrations and temperature distributions in all three phases are captured clearly with the GAFLOW-MPI. It demonstrates that the GASFLOW-MPI can accurately described the details of the related hydrogen behaviors in the accident and management process in the confined enclosure like the NPP. This paper can provide guidance for the numerical computation of the hydrogen safety issues in the confined space.

Introduction

Hydrogen behaviors in confined enclosure

Hydrogen plays a key role as an environment friendly and promising energy carrier in the near future energy systems [2,6,26]. Currently, much attention has been attached to the practical applications and scenarios with the confined enclosure such as the hydrogen fuel cell vehicles [5,13], refueling station [12,27], containment of the nuclear power plant (NPP) [7,15], and so on [18]. However, the hydrogen release in the confined enclosure is of great concern due to its easy leakage, high buoyancy, diffusion, low-energy ignition and a wide range of combustible hydrogen-air mixtures [21]. Especially, the hydrogen behaviors in the confined enclosure like the NPP containment are of enormous interest as they contribute to the early containment failure in the Fukushima NPP accident [7,15].

Therefore, an accurate prediction of these hydrogen behaviors in the accident and management process is a crucial topic for both the hydrogen safety assessment and containment safety analysis in the confined enclosure [15]. In the accident and management process, the hydrogen release, stratification and dissolution consequently occur. Meanwhile, the major safety issues are the distribution and mixing of the hydrogen in the containment atmosphere. It can present a risk for a fast deflagration and associated high pressure loads on the structures of the containment.

On the one hand, the experiments in the real-world applications are rather costing and time-consuming [3,10]. On the other hand, the supplementation or even the replacement of experiments by the CFD is of promising direction in industrial fields. Hence, the computational fluid dynamic (CFD) is gradually gaining acceptance as a power tool to analyze the hydrogen behaviors in the confined enclosure.

Helium adopted for hydrogen

Confidence in the calculation of the CFD depends on the validation of their results against the relevant experiment data. Due to safety issues, the majority of the hydrogen experiments are limited to small sizes or physical-scaled analogues [23,27]. In order to eliminate the accidental hydrogen combustion in the large-size experiment facilities especially in the confined space, the light gas helium is commonly adopted as a substitute due to the similar densities of two gases [3,9,22,23,32].

To ensure the similarity of two gases, the correlation of the equivalent volume flow rate between the helium and hydrogen is presented in Eq. (1) [14]. In Eq. (1), the parameter n is determined with the equal concentration ($n = 0.5$), equal volume flow rate ($n = 0$) and equal buoyancy ($n = 1$) respectively. It is suggested that the equal volume flow rate ($n = 0$) condition generally illustrates a reasonable similarity over the gas release and at various regions [14]. Therefore, the helium can be also adopted as a surrogate gas to conduct the research of the hydrogen behavior like the above recent studies.

$$Q_{He} = Q_{H_2}\left[\frac{(\rho_{air} \quad \rho_{He})}{(\rho_{air} \quad \rho_{H_2})}\right]^n \tag{1}$$

where Q_{He} is the volume flow rate of the helium, m^3/s; Q_{H2} is the volume flow rate of the hydrogen, m^3/s; ρ_{air}, ρ_{He} and ρ_{H_2} are the air density, helium density and hydrogen density respectively.

Germany THAI test

The Germany thermal-hydraulics, hydrogen, aerosols and iodine project (THAI) conducts a series of experiments like the TH21, TH22 and TH24 to predict the phenomena which may occur in a NPP containment in case of the accident scenario [7,10,11,15,17]. In which, the hydrogen behaviors like the hydrogen transportation and mixing in the confined enclosure is one of the main concerned safety issues.

Among them, the particular objective of the TH22 test facility is to study the hydrogen release, stratification and dissolution in the accident scenario [10,15] in the NPP. It is to investigate conditions about the dissolution of a light gas cloud in the upper plenum of the vessel by the natural convective flow. Consequently, the experiments performed in the THAI test series including the TH22 provide a unique data pool for the assessment and validation of both the lumped

parameter code and CFD codes with 3-D capabilities. In the TH22 test facility, the light gas helium is adopted as a substitute for hydrogen.

GASFLOW-MPI CFD code

Initially, lumped parameter codes have been used for the hydrogen behaviors in the confined enclosure [16,17]. However, it can hardly describe the detail information of both the thermal hydraulics and hydrogen behaviors in the hydrogen accident scenario. Hence, a CFD code with 3-D capabilities is necessary to capture the hydrogen behaviors in the NPP containment.

In the past decades, the 3-D parallel CFD code GASFLOW-MPI has been well behaved for the prediction in the large-scale test facilities like the HDR (T31.5, E11.2) [24], THAI (HM-1, HM-2, TH20) [24,41], MISTRA (ISP47) [1], TOSQAN (ISP47) [1], etc. It relies on the compressible Navier-Stokes equations and all-speed Arbitrary-Lagrangian-Eulerian (ALE) method. Hence, it can cover many scientific issues and engineering applications [18,19,34,37,42] related to the hydrogen behaviors.

Especially, GASFLOW-MPI is a well validated parallel CFD code which focuses on the thermal hydraulics and hydrogen behaviors (hydrogen release, dispersion, transportation, mixing, combustion, etc.) of the confined space [17,33,38–41]. Therefore, the hydrogen behaviors including the transient light gas release, stratification and dissolution in the TH22 test facility for the confined space like the NPP containment are analyzed and compared using the 3-D parallel CFD code GASFLOW-MPI. It should be noted that the light gas helium is adopted as a substitute for the hydrogen in the calculations in accordance with the experiment [10].

Scope of this paper

An accurate prediction related to the hydrogen behaviors in the accident and management process is indispensable for the hydrogen safety assessment in the confined enclosure. Therefore, the hydrogen behaviors including the transient light gas release, stratification and dissolution in the TH22 test facility for the confined enclosure like the NPP containment are analyzed and compared using the 3-D CFD code GASFLOW-MPI in this paper. In particular, the light gas helium is adopted as a substitute for the hydrogen in accordance with the experiment. In Section Model and setup, firstly, the detached eddy simulation (DES) turbulence model in the GASFLOW-MPI is introduced; then, the numerical model and experiment setup of the TH22 test facility are illustrated, including the geometry model, the initial and boundary conditions, the experiment setup and measurement. In Section Results and discussion, the hydrogen behaviors including the light gas release, stratification and dissolution are analyzed and validated with the experiment data. In addition, the velocity profiles, light gas concentrations, dimensionless numbers and temperature distributions are evaluated for the characteristics of the hydrogen behaviors. Section Conclusions comes to the conclusions and remarks on the numerical simulation in the TH22 test facility.

Model and setup

DES turbulence model

For the accurate prediction on the hydrogen behaviors in the confined space, the turbulence model is a critical model in the 3-D CFD code. However, the commonly adopted Reynolds-averaged Navier–Stokes (RANS) model for the thermal hydraulics in the confined space only describe the average physical parameters and the unsteady turbulence fluctuations are hence ignored [36].

Additionally, the DES model is a hybrid turbulence model which makes a tradeoff between the large eddy simulation (LES) model and RANS model [39]. It can capture the details for the thermal hydraulics in the confined space with a suitable computation amount [20]. It was first proposed in 1997 [28]. In this paper, the Reynolds stress term is calculated with the DES model as shown in Eq. (2). Then, the turbulence kinetic energy k and turbulent dispassion rate are calculated with Eqs. (3) and (4). Especially, the turbulence length scale l_{des} in the DES model can switch from the standard k-ε RANS model to the LES model automatically with Eqs. (5) and (6). Moreover, the DES model attempts to treat the near-wall regions with the RANS method, and treat the rest flow areas with the LES manner. The parameters used in the DES model are shown in Table 1.

$$\tilde{\sigma}_{ij} = 2\mu_t\left(S_{ij} \quad \frac{1}{3}S_{kk}\delta_{ij}\right) \tag{2a}$$

$$\mu_t = \rho C_\mu \frac{k^2}{\varepsilon} \tag{2b}$$

where S is the strain rate tensor, μ_t is the turbulent viscosity coefficient.

$$\frac{\partial}{\partial t}(\rho k) + \nabla\cdot(\rho k\mathbf{U}) = \nabla\cdot\left[\left(\mu + \frac{\mu_t}{\sigma_k}\right)\nabla k\right] + G_k + G_b \quad \frac{\rho k^{3/2}}{l_{des}} \tag{3}$$

$$\frac{\partial}{\partial t}(\rho \varepsilon) + \nabla\cdot(\rho \varepsilon\mathbf{U}) = \nabla\cdot\left[\left(\mu + \frac{\mu_t}{\sigma_\varepsilon}\right)\nabla \varepsilon\right] + C_1\frac{\varepsilon}{k}(G_k + G_b) \quad C_2\rho\frac{\varepsilon^2}{k} \tag{4}$$

$$l_{des} = \min(l_{rke}, l_{les}) \tag{5}$$

$$l_{rke} = \frac{k^{3/2}}{\varepsilon}, l_{les} = C_{des}\Delta_{max}, \Delta_{max} = \max(\Delta x, \Delta y, \Delta z) \tag{6}$$

where l_{rke} and l_{les} are the turbulence length scale of the standard k-ε model and LES model respectively; G_b is the buoyancy effect term.

Furthermore, the helium concentration with the LES, DES and RANS model in the GASFLOW-MPI during the time $t = 600$ s–1400 s are compared with the experiment data in the position of the sensor 207 (x = y = 0 m, z = 7.7 m) in Fig. 1.

Table 1 – Parameters used in the DES model.

C_1	C_2	C_μ	C_{des}	σ_k	σ_ε
1.44	1.92	0.09	0.65	1.0	1.3

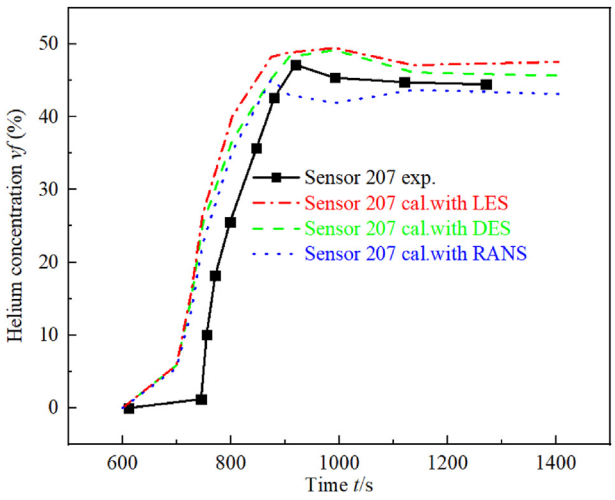

Fig. 1 – Model comparison of the light gas concentrations *vf* in the vessel with the experiment and calculation data in the position of sensor 207 during the time *t* = 600s–1400s.

Although the relative error is large due to the small value of the light gas concentration in the gas release and stratification period (the relative error will be discussed in Section Validation of GASFLOW-MPI with experiment data), the calculation results with the DES model are almost in the range of that with the LES and RANS model. It is relatively closer to the experiment data especially during the time $t > 900$s. This demonstrates that the DES model could has better performance in the confined space like the NPP containment.

In addition, the DES model has been better validated than the RANS model against the experiment data in the field of the thermal hydraulics and hydrogen behaviors in the confined enclosure like the NPP containment [4]. Both the term in the DES model and the DES model itself have been widely validated by the international benchmarks using the GASFLOW-MPI [35,39–41]. Consequently, the numerical calculations are carried out with the DES model in the GASFLOW-MPI CFD code.

Numerical model and boundary conditions

In this part, a Cartesian 3-D geometry model for the TH22 test facility was constructed with the GASFLOW-MPI code as shown in Fig. 2. In order to obtain the detail hydrogen behaviors of the TH22 test facility with an acceptable computational resource especially in the upper part of the vessel, the mesh size should be proper.

For the grid independence issue, three mesh sizes with 34×34×258, 68×68×258 and 68×68×516 are analyzed for the light gas concentration in the position of sensor 207 at the time $t = 800$ s. According to the calculation result, the light gas concentration *vf* are 35.2%, 36.8% and 37.1% respectively. The relative errors are 4.3% and 0.7%. In order to obtain both the nice accuracy and efficiency, the mesh size of 68×68×258 is selected in the calculation. In Fig. 2(a), the total mesh size in the GASFLOW-MPI for the TH22 test facility is 68×68×258≈1,200,000. In this geometry model, a variable mesh size method is applied. It was nearly uniform in the x, y axis direction while the variable mesh size was adopted in the z axis direction. Additionally, the minimum mesh size in the x, y and z axis direction of the geometry model is 5.83 cm, 5.83 cm and 3.05 cm respectively. From Fig. 2(b), the mesh difference between the adjacent cell in the variable mesh area is within 15% to ensure the high-quality mesh.

In particular, the inlet velocity magnitudes v_m at the nozzle is around 3.20 m/s (see Fig. 9(a) in Section Phase II: light gas release and stratification), which agrees well with the theoretical inlet velocity 3.21 m/s at the nozzle. This consistency between the calculated velocity and theoretical value also indicates that mesh resolution and time step size is also fine enough to meet the requirements for the DES model.

The test conditions and parameters in the TH22 test facility are given in Table 2 [10,15]. In Table 2, the fluid temperature in the vessel is 363.15 K. In addition, the wall temperature of the cold walls and hot walls are constant 313.15 K and 393.15 K respectively. Furthermore, the light gas helium is injected during time $t = 600$ s–800 s with a mass flowrate of 8 g/s. The gas pressure is 1.22 bar in both the vessel and the nozzle.

In according to the experiment, the simulation procedures can be classified into three phases [10,15]: (1) Phase I: establishment of the natural convection ($t = 0$–600 s); (2) Phase II: light gas release and stratification ($t = 600$ s–800 s); (3) Phase III: dissolution of the light gas cloud ($t = 800$ s–4000 s).

TH22 test facility setup

The TH22 test investigates the hydrogen release, stratification and dissolution of the THAI test vessel [10,15]. In Fig. 3, the TH22 test facility is a cylindrical vessel with 9.2 m in heigh and 3.2 m in diameter. Its volume is 60 m^3.

For the hydrogen behaviors experiment, the inner cylinder is installed in the TH22 test facility as shown in Fig. 3(a). For the light gas helium injection, a vertical injection nozzle of 138 mm (0.138 m) in diameter was implemented at the position of the height $z_{inlet} = 6.8$ m, radius $r = 1.14$ m and angle $\phi = 70°$. The research objective of the TH22 test facility is to mainly investigate the dissolution of a light gas cloud in the upper plenum of the vessel by the natural convective flow. In the TH22 test facility, the lower and middle vessel mantles are heated to a constant temperature 393.15 K, while the upper mantel is cooled with a constant temperature 313.15 K.

Measurement

Test instrumentation and accompanying data acquisition systems are used in test TH22 for the online control of vessel conditioning (wall heating/cooling). The thermal hydraulic conditions in the vessel and measurement sensors for the light gas injection, evolution of the light gas concentration during the test as shown in Fig. 3(b) [10,15].

Firstly, the volumetric flow rate of the light gas is measured with a rotameter type transducer originally designed for steam. Secondly, the calibrated 1.5-mm thermocouples for the temperature measurement (accuracy ±0.3 K) are positioned at the specified locations inside the test vessel. Thirdly, two strain-gauge type pressure transducers are installed to measure the quasi-steady vessel pressure during the experiment (accuracy ±4 mbar or ±6 mbar). Fourthly, the local light gas

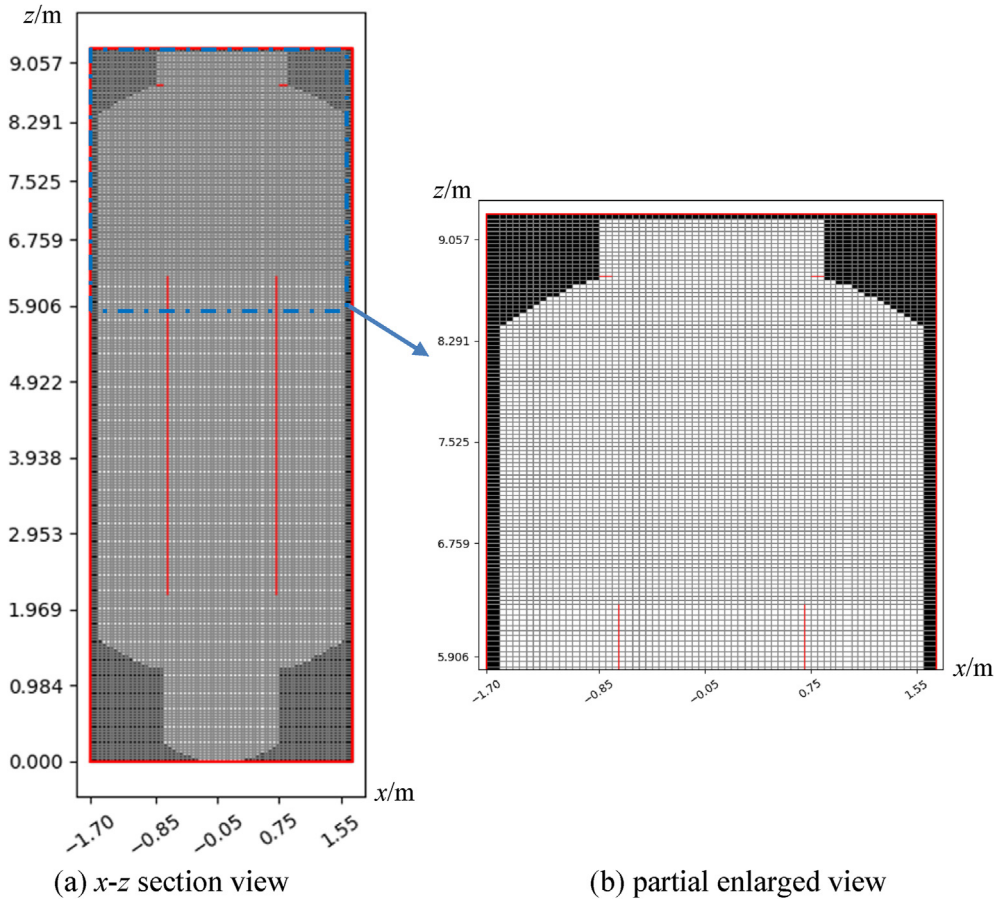

Fig. 2 – Illustration of numerical mode with GASFLOW-MPI. (a) *x*-zsection view (b) partial enlarged view.

concentrations of 15 locations in the vessel are measured by a continuous sampling system (thermal conductivity sensors). In order to improve the concentration measurement of gas mixtures in the vessel, a mass spectrometer is installed for the current and further research that allows on-line measuring of the air, light gas and steam concentrations via 40 sampling channels. Fifthly, five vane-wheel sensors in Fig. 3(b) are installed in the THAI vessel to measure gas velocity at the selected locations. At the same time, a particle-image velocimeter is applied to monitor the flow field prior to and during the erosion of the light gas cloud. The details of the measurement instruments are shown in Fig. 3.

Results and discussion

In the TH22 test facility, there are three phases of the hydrogen behaviors in the accident and management process: (1) Phase I: establishment of the natural convection (t = 0–600 s); (2) Phase II: light gas release and stratification (t = 600 s–800 s); (3) Phase III: dissolution of the light gas cloud (t = 800 s–4000 s). From the definition of validation, it is the process of obtaining the degree to which a model is accurately consistent with the real world [25]. Before analysis on the three phases in the light gas release, stratification and dissolution process, the validation of GASFLOW-MPI with the experiment data is hence illustrated.

Validation of GASFLOW-MPI with experiment data

Comprehensive comparisons of the light gas concentrations *vf* between the experiment data and calculation results in all three phases are shown in Fig. 4. From Fig. 4, the light gas concentration in the sensor 205, sensor 207, sensor 202 and sensor 201 are in the z position of 6.3 m, 7.7 m, 8.4 m and 9 m in the vessel centerline respectively. Especially, the sensor 209 is in the same $x = 0.55$ m plane of the injection nozzle while the opposite direction in the y axis of the injection nozzle with $y = 0.98$ m and $z = 7.7$ m. Moreover, the error analysis between the experiment and simulation data in the positions of five sensors are presented in Fig. 5.

In Fig. 5, the calculated light gas volume fraction *vf* in the position of the sensor 205 ($x = y = 0$ m, $z = 6.3$ m) agrees well with the experimental data during the light gas release and stratification period (t = 600 s–800 s). Meanwhile, the calculated light gas concentrations *vf* are mostly slightly higher than that of the experiment data. It should be noted that there is a time delay between the calculation result and the experiment data (See Fig. 1 in Section DES turbulence model) during this period. This will lead to a large relative error due to the

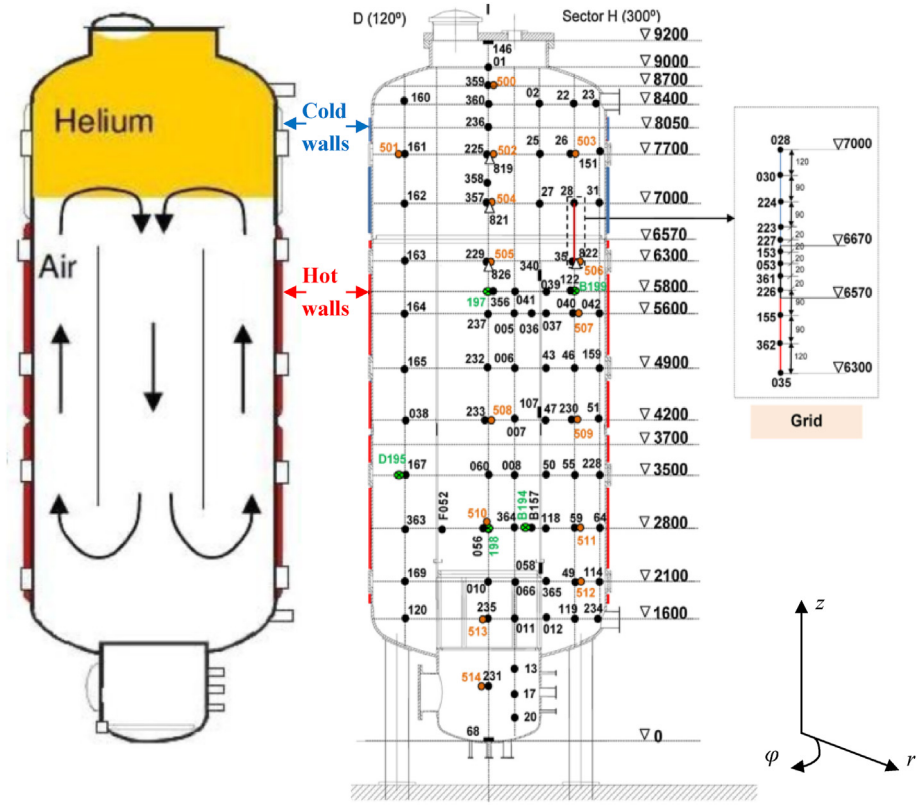

Fig. 3 – Configuration and instrumentation of the TH22 test facility [10,15]. (a) configuration (b) instrumentation.

small value of the light gas concentration in the initial injection of this phase. At the same time, a small measurement fluctuation would lead to large error in this period. Hence, it is reasonable to consider the relative error after the Phase II.

For the relative error in the phase III, it reaches the maximum relative error around the time t = 3370s. At the time t = 3370s, the calculated and experimental light gas concentrations *vf* are 12.62%, 14.11% respectively. Hence, the relative error during this period is within 11.9% in Fig. 5(a). Due to the small experimental value at the position of the sensor 205, the maximum relative error is large in some degree. In fact, the maximum absolute error is 1.5% of the light gas concentration.

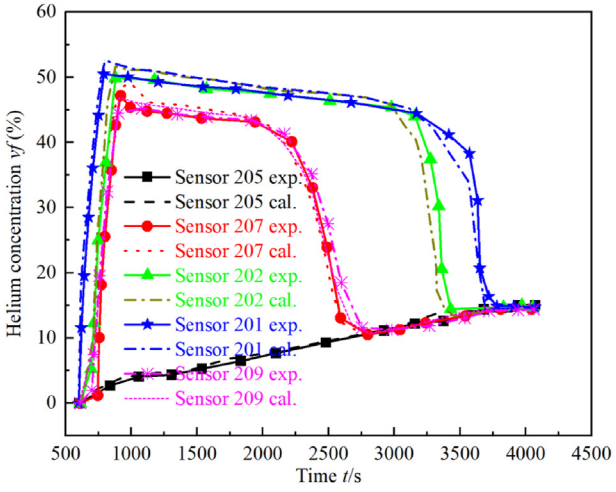

Fig. 4 – Comparison of the light gas concentrations *vf* in the vessel with the experiment and calculation data in five sensors with Phase I (establishment of the natural convection, t = 0–600 s), Phase II (light gas release and stratification, t = 600 s–800 s), Phase III (dissolution of the light gas cloud, t = 800 s–4000 s).

As the light gas release at the position of height z = 6.8 m, the sensor 207 (x = y = 0 m, z = 7.7 m), sensor 202 (x = y = 0 m, z = 8.4 m) and sensor 201 (x = y = 0 m, z = 9.0 m) are in the upper space from the injection nozzle. In Fig. 5(b), the calculated light gas concentrations *vf* in the position of the sensor 207, sensor 202 and sensor 201 are consistent with the experimental data during the light gas release and stratification period (t = 600 s–800 s). Similarly, the calculated light gas concentrations *vf* are a little larger than that of the experiment data in this phase. Therefore, the relative error in the light gas dissolution phase (t > 800 s) is less than 4.2% in Fig. 5(b).

Furthermore, the sensor 209 are in the position of x = 0.55 m, y = 0.98 m and z = 7.7 m. In Fig. 5(c), the calculated light gas concentration *vf* in the position of the sensor 209 coincides with the experimental data during the dissolution of the light gas cloud period (t > 800 s). Additionally, the calculated light gas concentrations *vf* slightly overestimate than that of the experiment in this phase. Moreover, the relative error during this period is within 3.6%.

As the time for the complete dissolution, it coincides with the experiment data from Figs. 4 and 5. Then, the relative errors of the time for the complete dissolution between the calculation results and experiment data are within 5.0%.

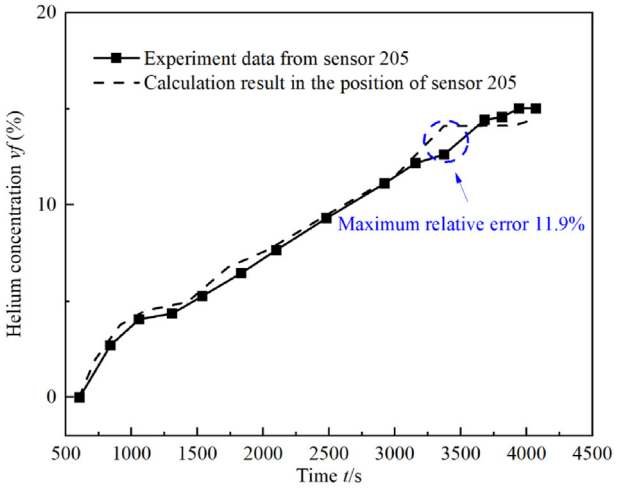

(a) in the position of the sensor 205

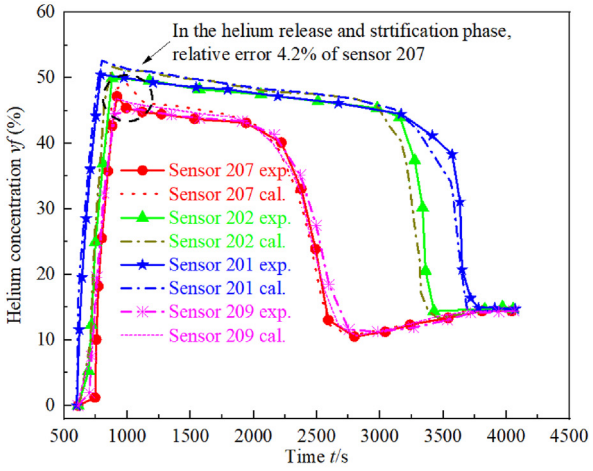

(b) in the positions of the sensor 207, sensor 202 and sensor 201

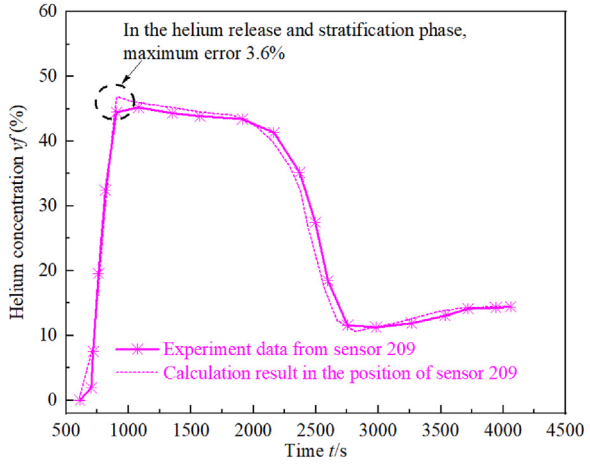

(c) in the position of the sensor 209

Fig. 5 – Comparison and error of the light gas concentrations *vf* in the vessel with the experiment and calculation data in the positions of five sensors. (a) in the position of the sensor 205 (b) in the positions of the sensor 207, sensor 202 and sensor 201 (c) in the position of the sensor 209.

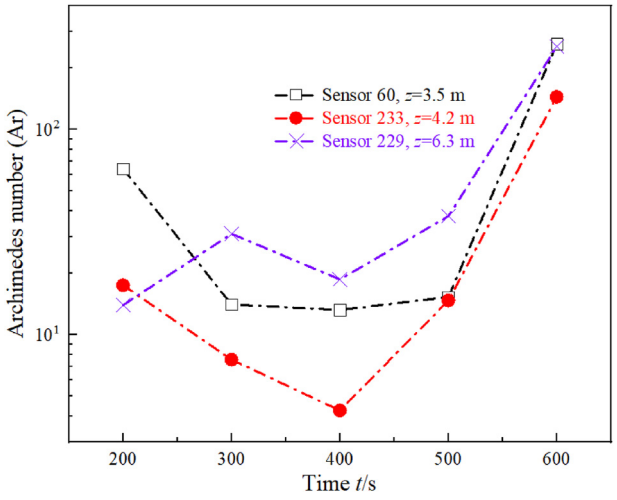

Fig. 6 – Variation of the Ar number with the time t before the light gas injection.

Among them, GASFLOW-MPI CFD code shows good agreements with the experiment data in the light gas release, stratification and dissolution process. It should be noted that the tendencies of the calculation results are slightly ahead of the experimental result in the light gas dissolution phase in Figs. 4 and 5. This may due to the slightly large value of the heat-transfer coefficient that applied to the convection [31].

Therefore, the relative errors in all sensor positions during the phase of the dissolution of the light gas cloud are within 11.9%. Except that in the position of the sensor 205, the relative errors in the positions of other four sensors (sensor 207, sensor 202, sensor 201, sensor 209) are both within 4.2%. At the same time, the relative errors of the time for the complete dissolution between the calculation results and experiment data are within 5.0%. Generally, the calculation results agree well with the experiment data. Hence, it fully illustrates that the GASFLOW-MPI can accurately predict the details of the hydrogen behaviors in the TH22 test vessel for the NPP.

Phase I: establishment of the natural convection

In this phase, it consists of the establishment of the natural convection by the temperature difference with the cold walls and hot walls. As the heated mantles of the vessel has been keep at 393.15 K for a long time before the start of the experiment, it may exist the initial velocity at the beginning of the experiment. Hence, the mixed convection of the fluid may exist.

In particular, the Archimedes number (Ar) in Eq. (7) is adopted to determine whether the natural convection dominates (Ar»1) or not (Ar«1) [30].

$$\mathrm{Ar} = \beta g h (T_{fh} \quad T_{fc}) / v_{inlet}^2 \tag{7}$$

where β is the surface thermal expansion coefficient, 1/K; g is the gravity acceleration constant, 9.8 m/s^2; T_{fh} and T_{fc} are the average fluid temperature near the hot and cold mantles respectively, K; v_{inlet} is the inlet fluid velocity, m/s.

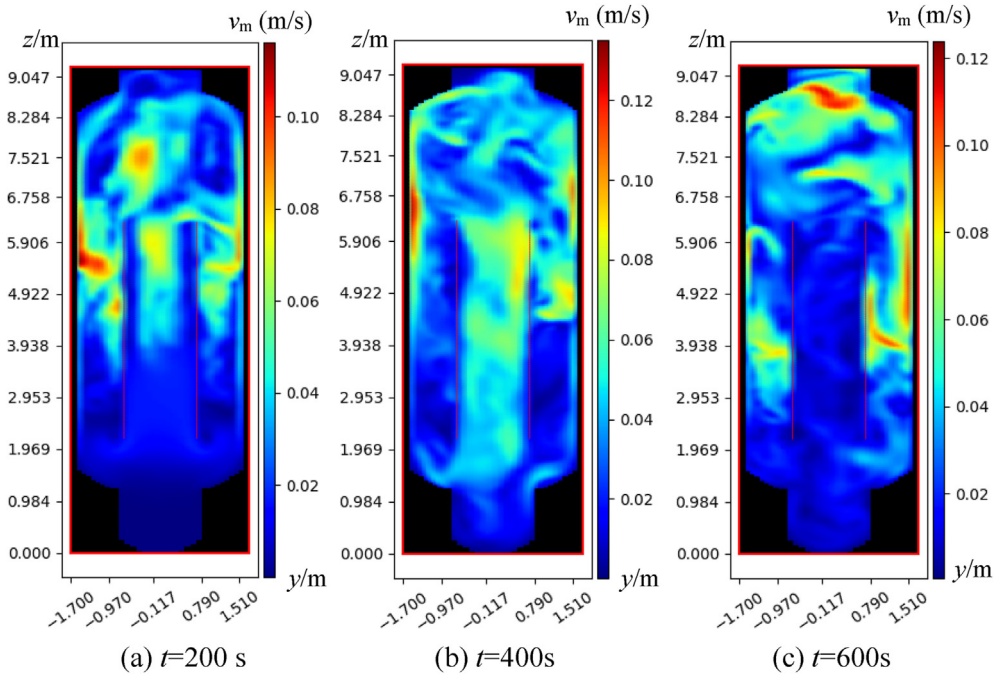

Fig. 7 – Variation of the velocity magnitude v_m before the light gas injection at $t = 200–600$ s at the $x = 0$ cross section. (a) t=200 s (b)t=400s (c)t=600s.

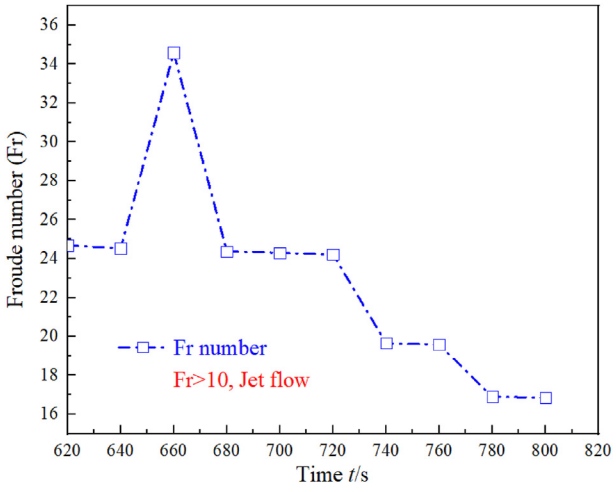

Fig. 8 – Variation of the Fr number during the light gas injection (t = 600 s–800 s).

During the phase I, the relative error between the calculation result and experiment data is quite small. Taken the sensor 60 with a position of z = 3.5 m for example, the calculation temperature ranges from 363.01 K to 363.02 K while the experiment data is from 363.00 K to 363.77 K at the time t = 0–600s. Its maximum relative error is within 0.3%. Hence, the accuracy of GASFLOW-MPI CFD code has been verified to a certain extent.

From Eq. (7), the Ar number is related with T_{fh} and T_{fc}. Nevertheless, the values of T_{fh} and T_{fc} in the confined space change with time. Based on the calculation result with the GASFLOW-MPI, the variation of the Ar number with the time t is presented in Fig. 6. From Fig. 6, the Ar number is always greater than 4 during the time t = 200 s–600 s in the phase I. At t = 600 s, the Ar numbers even exceed 100 in all three sensor positions. This fully proves that it is already dominated by the natural convection in the TH22 test vessel when t exceeds 200 s in the phase I. Moreover, the profiles of the velocity magnitude v_m in the TH22 test vessel are also shown in Fig. 7 at t = 200 s–600 s at the x = 0 cross section. Especially, the establishment of the natural convection by the temperature difference can be seen clearly in Fig. 7(a) and (b).

Phase II: light gas release and stratification

Helium is released upward in the TH22 test vessel and accumulates within the vessel due to the density difference between the light gas and air. Meanwhile, the motion of the inject light gas is determined by the inlet momentum and buoyancy force in the phase of the light gas release and stratification. Under these circumstances, the Froude number (Fr) in Eq. (8) is adopted to evaluate whether the jet flow (Fr > 10) or plume flow dominates (Fr < 10) [29].

$$Fr = v_{inlet}/(gD(\rho_\infty \quad \rho_{inlet})/\rho_{inlet})^{1/2} \tag{8}$$

where D is the inject nozzle diameter, m; v_{inlet} is the inject velocity, m/s; ρ_∞ is the far field ambient density, kg/m^3; ρ_{inlet} is the inlet or inject light gas density, kg/m^3.

Similarly in Eq. (8), the Fr number varies with the far field ambient density ρ_∞ while the ρ_∞ also change with the time t in the confined enclosure. Consequently, the variation of the Fr number with the time t should be presented as shown in Fig. 8. From Fig. 8, the Fr number exceeds 10 in the light gas release and stratification phase. Therefore, it belongs to the jet flow.

In addition, the calculated instantaneous light gas volume fraction distribution and velocity profile of a x = 0.55 m plane

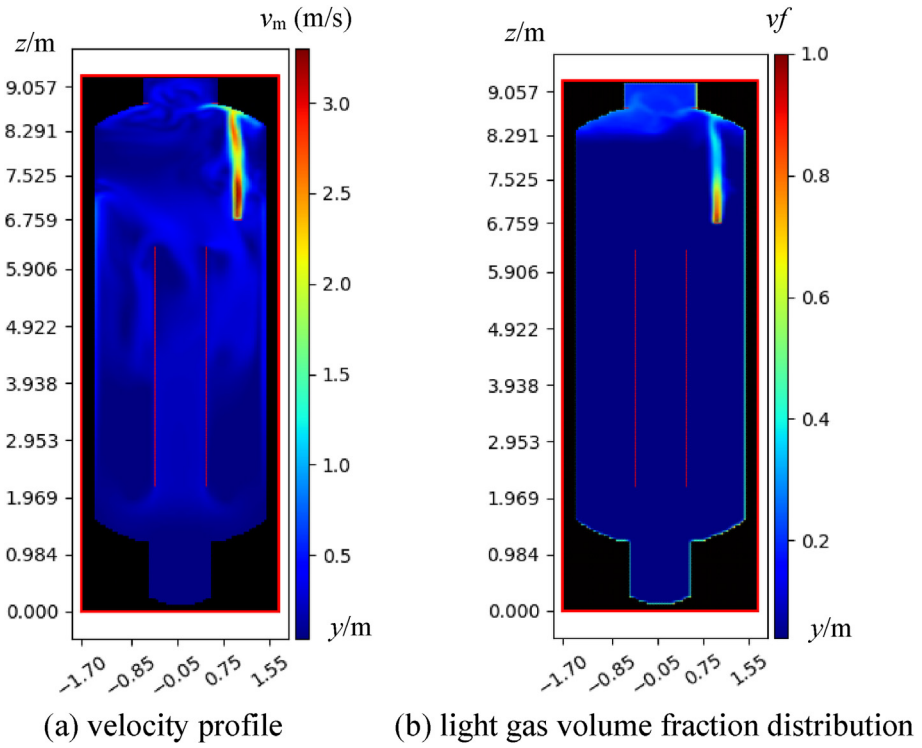

Fig. 9 – Calculated instantaneous velocity profile and light gas volume distribution of the $x = 0.55$ m plane at $t = 620$ s. (a) velocity profile (b) light gas volume fraction distribution

Table 2 – Initial and boundary conditions for the TH22 test facility.

Initial conditions			Boundary conditions		
Vessel fluid condition	Temperature of cold wall (K)	Temperature of hot wall (K)	Duration of Helium injection (s)	Helium Mass flow rate (g/s)	Nozzle helium condition
363.15 K, 1.22 bar	313.15 (constant)	393.15 (constant)	200 (t 600 s–800 s)	8	363.15 K, 1.22 bar

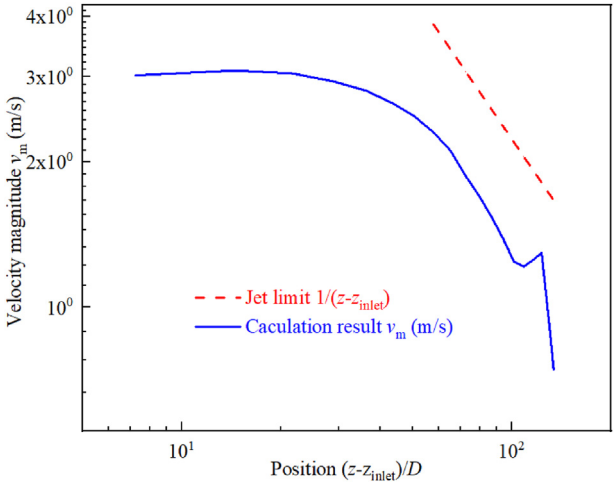

Fig. 10 – Averaged centerline velocity profile of the $x = 0.55$ m plane at $t = 620$ s.

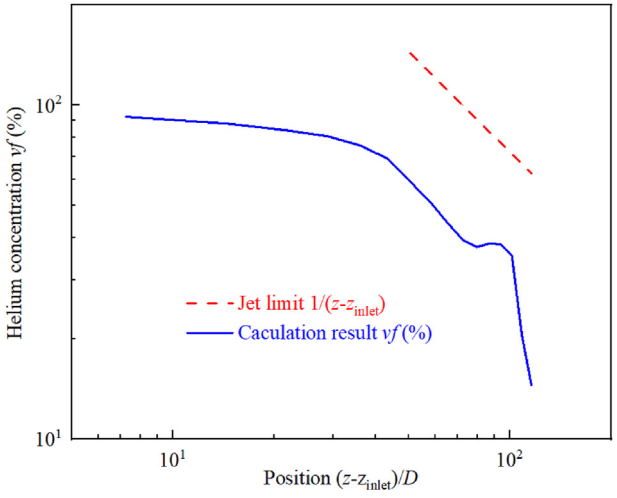

Fig. 11 – Averaged centerline light gas volume fraction distribution of the $x = 0.55$ m plane at $t = 620$ s.

at $t = 620$ s are shown in Fig. 9. Furthermore, the time averaged centerline velocity profile of the jet flow of the $x = 0.55$ m plane is shown in Fig. 10. In Fig. 10, the length of the potential core region is around 20 D. Afterwards, the velocity and light gas concentration decay with a slop of 1/z as shown. It coincides with the theoretical jet limit [39].

Similarly, the time averaged centerline light gas concentration distribution of a $x = 0.55$ m plane of the jet flow is presented in Fig. 11. In Fig. 11, the light gas volume fraction *vf* slightly decreases near the injection nozzle. Then, it descends with a certain slope of 1/z. which also matches the theoretical jet limit. Therefore, the time averaged centerline velocity and light gas concentration after the potential core region agrees well with the theoretical jet limit [29].

For the formation of the light gas stratification, there are four typical regions in the upward jet flow in the light gas release process, namely the core potential region, transition region, fully turbulence development region and impinging region. In the core potential region, it is the laminar flow near the injection nozzle. At this region, the time averaged centerline velocity and light gas concentration almost keep constant as shown in Figs. 10 and 11. Then, the transition region occurs at the end of the core potential region. It is the transition from the laminar flow to the turbulence flow with the shear force between the injection light gas and the air. Afterwards, the jet flow enters the fully development turbulence region. In the fully development turbulence region, the time averaged centerline velocity and light gas concentration decay with the lope of 1/z which are consistent with the theoretical jet limit.

Moreover, the jet flow impinges the top wall of the confined enclosure and spreads in radius directions as presented in Fig. 9(a). Its velocity component in the z axis decreases and is transformed into the radial horizontal component. Hence, many eddies with different scales generate and the light gas is strongly mixed with the surrounding air in this region. Lastly, the light gas stratification forms due to the buoyancy and turbulence.

The evolution of the light gas concentration and velocity are presented in Figs. 12 and 13. At the end of the phase II, a light gas cloud stratification is formed in Fig. 12(c). From Figs. 12(a) and 13(a), the light gas beings to accumulate and temperature difference is small at $t = 620$ s. In Figs. 12(b) and 13(b), a light gas layer forms and the temperature increases in the vessel at $t = 700$ s. This means that the light gas in the upper space like the positions of the sensor 202 and sensor 201 will be accumulated soon. As the jet flow dominates, the light gas concentration increases sharply. This is consistent with the experiment data in Fig. 4 in SectionValidation of GASFLOW-MPI with experiment data.

From Figs. 12(c) and 13(c), the light gas concentration distribution is obvious while the temperature difference between the lower and upper space in the vessel increases at $t = 800$ s. In Figs. 12 and 13, the light gas concentrations and temperature distributions in the phase of light gas release and stratification are described clearly with the GAFLOW-MPI.

Phase III: dissolution of the light gas cloud

For the light gas dissolution phase ($t > 800$ s), the light gas concentration *vf* in the positions of the sensor 205, sensor 207, sensor 202 and sensor 201 decrease slowly, then drop sharply, and finally reach a stable value as shown in Figs. 4 and 5.

Most importantly, the time for complete dissolution of each sensor coincides with the experiment data. In addition, the relative error of the time for complete dissolution at the corresponding each sensor position between the calculation results and experiment data is within 5%.

Moreover, the light gas volume fractions *vf* before, during the dissolution and after the complete dissolution of the light gas cloud are given in Fig. 14(a)–(c). Correspondingly, the temperature *T* distributions before, during the dissolution and after the complete dissolution of the light gas cloud are presented in Fig. 15(a)–(c).

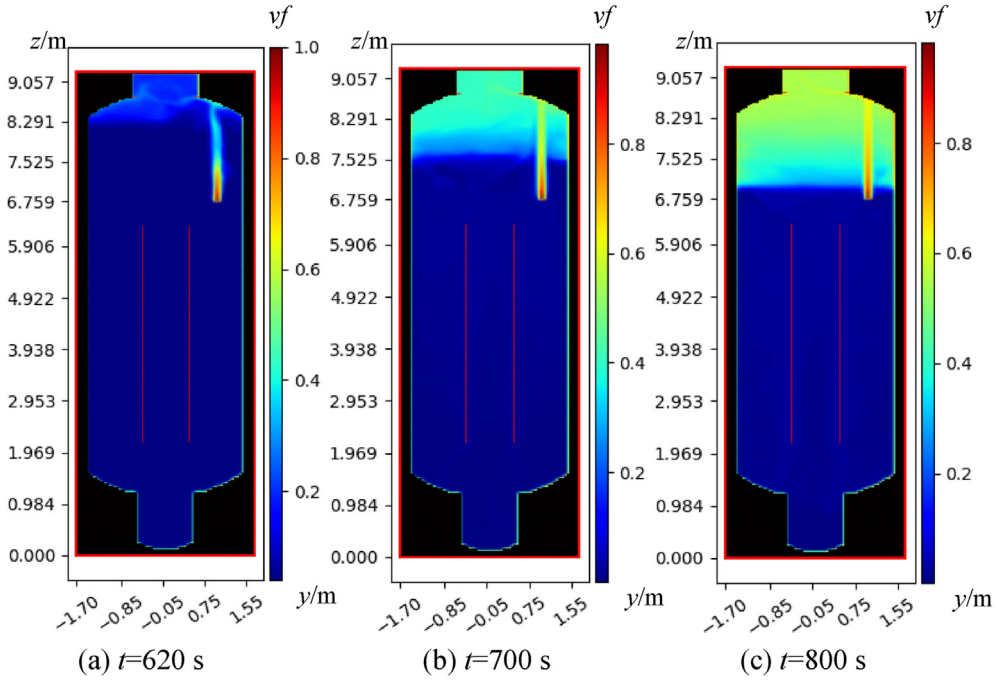

Fig. 12 – Calculated light gas concentration profiles of the $x = 0.55$ m plane at $t = 620$ s, 700 s and 800 s.

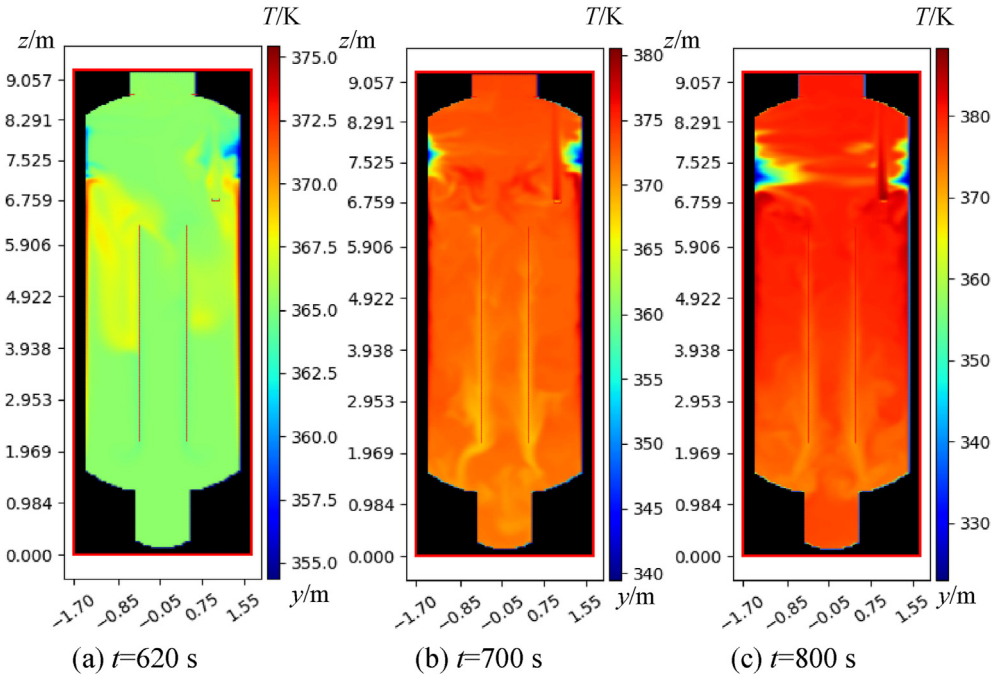

Fig. 13 – Calculated temperature distributions of the x = 0.55 m plane at t = 620 s, 700 s and 800 s.

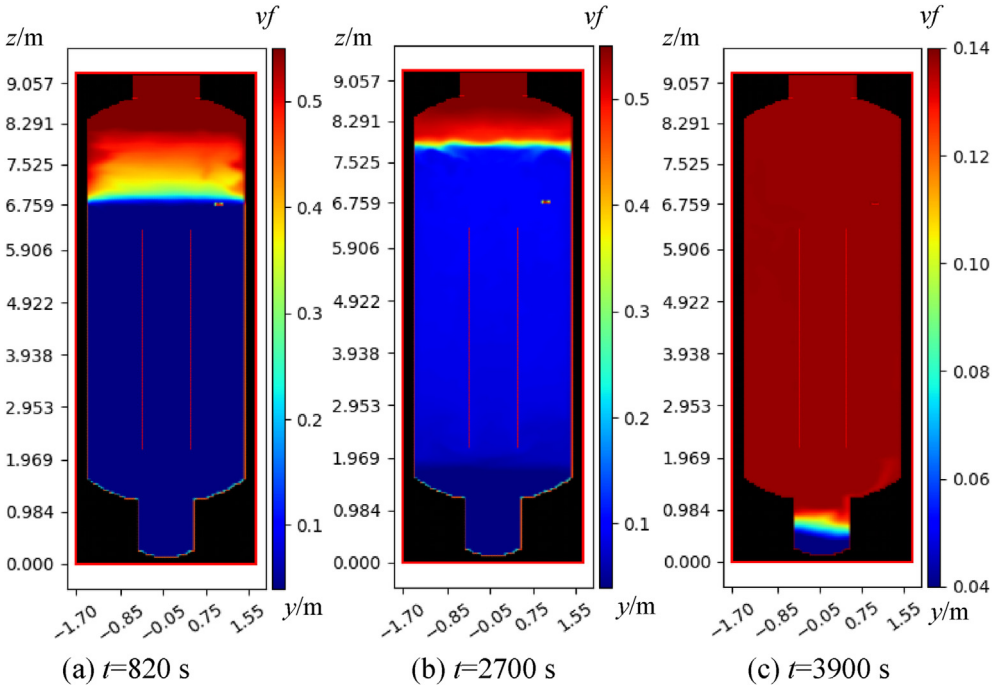

Fig. 14 – Calculated light gas concentration of the x = 0.55 m plane at t = 820 s, 2700 s and 3900 s.

Additionally, the Ar number in Eq. (7) is also adopted to determine whether the natural convection dominates (Ar»1) or not (Ar«1) [30]. For instance, the local Ar numbers in the position of the sensor 60 (z = 3.5 m), sensor 233 (z = 4.2 m) are 170 and 84 respectively at t = 2700 s with a reference position of the sensor 225 (z = 7.35 m). These Ar numbers far beyond 1 which means the natural convection already dominates at this time. From Figs. 4 and 5 in Section Validation of GASFLOW-MPI with experiment data, the light gas concentrations in the position of the sensor 207, sensor 209 had already decreased rapidly at t = 2700 s.

From Figs. 14(a) and 15(a), the dissolution of the light gas begins at t = 820 s. In Figs. 14(b) and 15(b), an obvious light gas layer is observed and the large temperature difference exists between the light gas cloud and lower space in the vessel at t = 2700 s. This means that the light gas in the upper space like

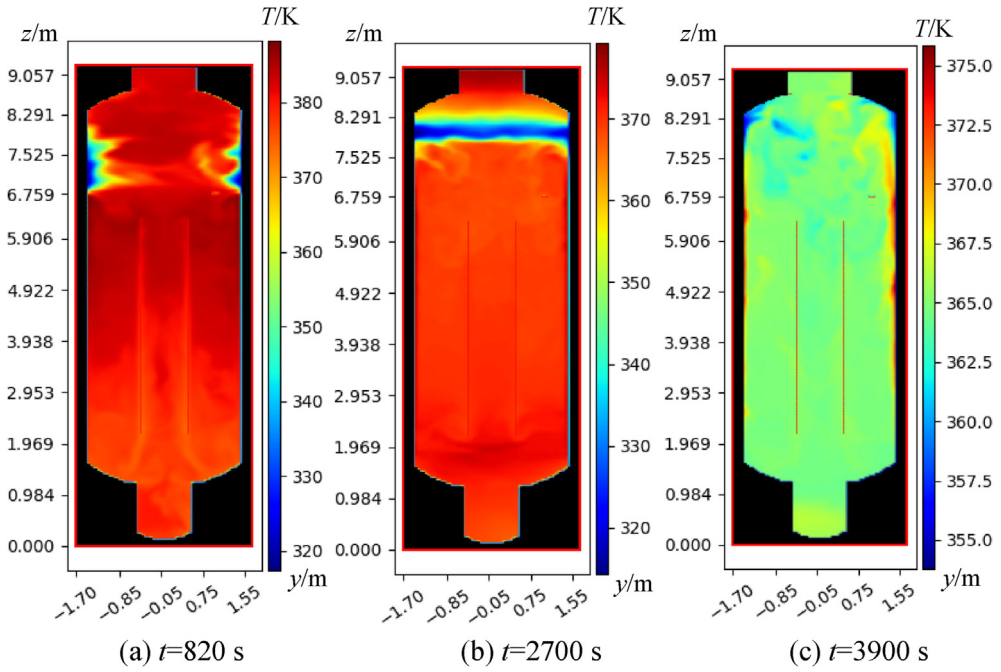

Fig. 15 − Calculated temperature distributions of the x = 0.55 m plane at t = 820 s, 2700 s and 3900 s.

the positions of the sensor 202 and sensor 201 will be diluted soon. Once the natural convection establishes and dominates, the light gas concentration decreases sharply. This is also consistent with the experiment data in Fig. 4 in Section Validation of GASFLOW-MPI with experiment data. From Figs. 14 (c) and 15(c), the light gas concentration distribution is relatively uniform while the temperature variation is small. In Figs. 14 and 15, the light gas concentrations and temperature distributions in the phase of the dissolution of the light gas cloud are illustrated clearly with the GAFLOW-MPI. It proves that the GASFLOW-MPI can detailly capture the dissolution of the light gas cloud with the natural convection in the vessel.

Conclusions

In this work, the hydrogen behaviors including the transient light gas release, stratification and dissolution in the TH22 test facility for the confined space like the NPP containment is analyzed and evaluated using the 3-D CFD code GASFLOW-MPI. Additionally, the light gas helium is adopted as a substitute for the hydrogen in the calculations in accordance with the experiment. Main conclusions are as below:

(1) Firstly, the calculation results are compared and validated with the experiment data. The relative errors between the calculation results and experiment data in all sensor positions during the phase III (the phase of the dissolution of the light gas cloud) are within 11.9%. Except that in the position of the sensor 205, the relative errors in the positions of other four sensors (sensor 207, sensor 202, sensor 201, sensor 209) in the phase III are both within 4.2%. In addition, the relative errors of the time for the complete dissolution between the calculation results and experiment data in the phase of the dissolution of the light gas cloud are within 5.0%.

(2) Then, the time averaged centerline velocity and light gas concentration after the potential core region decay with a slop of 1/z which agree well with the theoretical jet limit. The jet flow dominates as the Fr number exceeds 10 in the light gas release and stratification phase during the time t = 600 s−800 s.

(3) In addition, there are four typical regions in the upward jet flow in the light gas release process, namely the core potential region, transition region, fully turbulence development region and impinging region for the formation of the light gas stratification.

(4) Furthermore, the light gas concentrations and temperature distributions in the phase of the dissolution of the light gas cloud are captured clearly with the GAFLOW-MPI. As soon as the natural convection establishes and dominates, the light gas concentration decreases sharply.

(5) Lastly, this study demonstrates that the GASFLOW-MPI can accurately described the details of the related hydrogen behaviors in the accident and management process in the NPP.

An accurate prediction of these hydrogen behaviors in the accident and management process is a crucial topic for both the hydrogen safety assessment and safety analysis in the confined enclosure like the NPP containment. These findings can provide the guidance for researchers who aim to foster more research efforts in it.

Declaration of competing interest

The authors declare that they have no known competing financial interests or personal relationships that could have appeared to influence the work reported in this paper.

Acknowledgments

Acknowledgments for the experiment data provided by the report from the Research Management Division of the Gesellschaft für Anlagen-und Reaktorsicherheit (GRS) gGmbH for the article publication.

Nomenclature

Ar	The Archimedes number
CFD	The computational fluid dynamic
DES	The detached eddy simulation
Fr	The Froude number
LES	The large eddy simulation
NPP	The nuclear power plant
PIV	The particle-image velocimeter
RANS	The Reynolds-averaged Navier–Stokes
THAI	The thermal-hydraulics, hydrogen, aerosols and iodine project
D	The diameter of the injection nozzle, m or cm
G_b	The buoyancy effect term
g	The gravity acceleration constant, 9.8 m/s^2
k	The turbulent kinetic energy, m^2/s^2
l_{les}	The turbulence length scale of the standard LES model, m
l_{rke}	The turbulence length scale of the standard k-ε model, m
Q_{He}	The volume flow rate of the helium, m^3/s
Q_{H_2}	The volume flow rate of the hydrogen, m^3/s
r	The radius, m
S	The strain rate tensor
T	The temperature in the test vessel, K
T_{fc}	The average fluid temperature near the cold walls, K
T_{fh}	The average fluid temperature near the hot walls, K
t	The time, s
vf	The light gas concentration, %
v_m	The velocity magnitude, m/s
v_{inlet}	The inlet fluid velocity, m/s
x, y, z	The spatial coordinates, m
z_{inlet}	The height of the injection nozzle in the z coordinate, m
μ_t	The turbulent viscosity coefficient, Pa s
ε	The turbulent energy dissipation rate, m^2/s^3
ρ_∞	The ambient density, kg/m^3
ρ_{air}	The air density, kg/m^3
ρ_{H_2}	The hydrogen density, kg/m^3
ρ_{inlet}	The inlet or inject gas density, kg/m^3
β	The surface thermal expansion coefficient, 1/K
ϕ	The angle, rad or °

REFERENCES

[1] Allelein HJ, Schwarz S, Fischer K, et al. International standard problem ISP-47 on containment thermal hydraulics-Final report[R]. NEA/CSNI/R(2007)/10. Organisation for Economic Co-Operation and Development; 2007.

[2] Balat M. Potential importance of hydrogen as a future solution to environmental and transportation problems. Int J Hydrogen Energy 2008;33(15):4013–29.

[3] Chen M, Zhao M, Huang T, et al. Measurements of helium distributions in a scaled-down parking garage model for unintended releases from a fuel cell vehicle. Int J Hydrogen Energy 2020;45(41):22166–75.

[4] Ding P, Chen M, Li W, et al. CFD simulations in the nuclear containment using the DES turbulence models. Nucl Eng Des 2015;(287):1–10.

[5] Demirci UB, Akdim O, Andrieux J, et al. Sodium borohydride hydrolysis as hydrogen generator: issues, state of the art and applicability upstream from a fuel cell. Fuel Cell 2010;10(3):335–50.

[6] Demirci UB, Akdim O, Miele P. Ten-year efforts and a no-go recommendation for sodium borohydride for on-board automotive hydrogen storage. Int J Hydrogen Energy 2009;34(6):2638–45.

[7] Freitag M, Schmidt E, Gupta S, et al. Simulation benchmark based on Thai-experiment on dissolution of a steam stratification by natural convection. Nucl Eng Des 2016;(299):37–45.

[9] Gupta S, Brinster J, Studer E, et al. Hydrogen related risks within a private garage: concentration measurements in a realistic full scale experimental facility. Int J Hydrogen Energy 2009;34(14):5902–11.

[10] Gupta S, Fischer K, Langer G, et al. THAI test TH22, dissolution of a light gas stratification by natural convection [R]. Technical Report 1501361-TH22-TR. Eschborn, Germany: Becker Technologies GmbH; 2010.

[11] Gupta S, Schmidt E, Von LB, et al. Thai test facility for experimental research on hydrogen and fission product behavior in light water reactor containments. Nucl Eng Des 2015;(294):183–201.

[12] Gye HR, Seo SK, Bach QV, et al. Quantitative risk assessment of an urban hydrogen refueling station. Int J Hydrogen Energy 2019;44(2):1288–98.

[13] Hames Y, Kaya K, Baltacioglu E, et al. Analysis of the control strategies for fuel saving in the hydrogen fuel cell vehicles. Int J Hydrogen Energy 2018;43(23):10810–21.

[14] He J, Kokgil E, Wang LL, et al. Assessment of similarity relations using helium for prediction of hydrogen dispersion and safety in an enclosure. Int J Hydrogen Energy 2016;41(34):15388–98.

[15] Kelm S, Lehmkuhl J, Jahn W, et al. A comparative assessment of different experiments on buoyancy driven mixing processes by means of CFD. Ann Nucl Energy 2016;(93):50–7.

[16] Kim J, Lee U, Hong SW, et al. Spray effect on the behavior of hydrogen during severe accidents by a loss-of-coolant in the APR1400 containment. Int Commun Heat Mass Tran 2006;33(10):1207–16.

[17] Li Y, Zhang H, Xiao J, et al. Numerical investigation of natural convection inside the containment with recovering passive containment cooling system using GASFLOW-MPI. Ann Nucl Energy 2018;(114):1–10.

[18] Li Y, Xiao J, Zhang H, et al. Numerical analysis of hydrogen release, dispersion and combustion in a tunnel with fuel cell vehicles using all-speed CFD code GASFLOW-MPI. Int J Hydrogen Energy 2020. https://doi.org/10.1016/j.ijhydene.2020.09.063.

[19] Lyu X, Lee X, Ji K, et al. Impact of inert gas injection rate on reducing hydrogen risk during AP1000 post-inerting. Ann Nucl Energy 2017;(110):230–3.
[20] Mahaffy J, Chung B, Song C, et al. Best practice guidelines for the use of CFD in nuclear reactor safety applications-revision[R]. Organisation for Economic Co-Operation and Development; 2015.
[21] Malakhov AA, Avdeenkov AV, Du Toit MH, et al. CFD simulation and experimental study of a hydrogen leak in a semi-closed space with the purpose of risk mitigation. Int J Hydrogen Energy 2020;45(15):9231–40.
[22] Pitts WM, Yang JC, Blais M, et al. Dispersion and burning behavior of hydrogen released in a full-scale residential garage in the presence and absence of conventional automobiles. Int J Hydrogen Energy 2012a;37(22):17457–69.
[23] Pitts WM, Yang JC, Fernandez MG. Helium dispersion following release in a 1/4-scale two-car residential garage. Int J Hydrogen Energy 2012b;37(6):5286–98.
[24] Royl P, Lee UJ, Travis JR, et al. Benchmarking of the 3D CFD code GASFLOW II with containment thermal hydraulic tests from HDR and Thai. In: The CFD4NRS conference; September 5th-7th, 2006.
[25] Sargent RG. Verification and validation of simulation models. J Simulat 2013;7(1):12–24.
[26] Schlapbach L. Hydrogen-fuelled vehicles. Nature 2009;460(7257):809–11.
[27] Shirvill LC, Roberts TA, Royle M, et al. Safety studies on high-pressure hydrogen vehicle refuelling stations: releases into a simulated high-pressure dispensing area. Int J Hydrogen Energy 2012;37(8):6949–64.
[28] Spalart PR. Comments on the feasibility of LES for wings, and on a hybrid RANS/LES approach. In: Proceedings of 1st AFOSR international conference on DNS/LES. Greyden Press; 1997.
[29] Schefer RW, Houf WG, Williams TC. Investigation of small-scale unintended releases of hydrogen: buoyancy effects. Int J Hydrogen Energy 2008;33(17):4702–12.
[30] Spall RE. A numerical study of transient mixed convection in cylindrical thermal storage tanks. Int J Heat Mass Tran 1998;41(13):2003–11.
[31] Stewering J, Schramm B, Sonnenkalb M. Validation of CFD-codes for natural convection and condensation phenomena in containments with German Thai-experiments[C]. In: Proceedings of the international topical meeting on nuclear reactor thermal hydraulics, Chicago, United States; August 30-September 4, 2015.
[32] Swain MR, Filoso P, Grilliot ES, et al. Hydrogen leakage into simple geometric enclosures. Int J Hydrogen Energy 2003;28(2):229–48.
[33] Xiao J, Breitung W, Kuznetsov M, et al. A new 3-D parallel all-speed CFD code for turbulent dispersion and combustion simulations: Part I: models, verification and validation. Int J Hydrogen Energy 2017a;(42):8346–68.
[34] Xiao J, Breitung W, Kuznetsov M, et al. GASFLOW-MPI: a new 3-D parallel all-speed CFD code for turbulent dispersion and combustion simulations Part II: first analysis of the hydrogen explosion in Fukushima Daiichi Unit 1. Int J Hydrogen Energy 2017b;42(12):8369–81.
[35] Xiao J, Breitung W, Kuznetsov M, et al. Numerical investigations of turbulent slow deflagration of premixed H_2-air-H_2O mixture in Thai test HD-22 using CFD code GASFLOW-MPI. In: In17th international topical meeting on nuclear reactor thermal hydraulics. NURETH-17; 2017c.
[36] Xiao J, Travis JR, Royl P, et al. Three-dimensional all-speed CFD code for safety analysis of nuclear reactor containment: status of GASFLOW parallelization, model development, validation and application. Nucl Eng Des 2016;(301):290–310.
[37] Yu F, Zhang H, Li Y, et al. Voxelization-based high-efficiency mesh generation method for parallel CFD code GASFLOW-MPI. Ann Nucl Energy 2018;(117):277–89.
[38] Zhang H, Li Y, Xiao J, et al. Large eddy simulation of turbulent flow using the parallel computational fluid dynamics code GASFLOW-MPI. Nucl Eng Technol 2017;49(6):1310–7.
[39] Zhang H, Li Y, Xiao J, et al. Detached Eddy Simulation of hydrogen turbulent dispersion in nuclear containment compartment using GASFLOW-MPI. Int J Hydrogen Energy 2018a;43(29):13659–75.
[40] Zhang H, Li Y, Xiao J, et al. Uncertainty analysis of condensation heat transfer benchmark using CFD code GASFLOW-MPI. Nucl Eng Des 2018b;(340):308–17.
[41] Zhang H, Li Y, Xiao J, et al. Numerical study of the stratification erosion benchmark for NPPs containment using CFD code GASFLOW-MPI. Ann Nucl Energy 2019;(132):199–211.
[42] Zhang H, Sauerschell S, Ba Q, et al. Numerical simulation of accidental released hazardous gas dispersion at a methanation plant using GASFLOW-MPI. Int J Hydrogen Energy 2021;46(2):2804–23.